Journal of Sustainable Development of Energy, Water and Environment Systems

http://www.sdewes.org/jsdewes

Year 2026, Volume 14, Issue 2, 1140695

Original Research Article

Coupled Thermal and Optical Impact of Dust Thermophysical Properties on Solar Photovoltaic Performance

***Kudzanayi Chiteka*[*1], *Christopher C. Enweremadu*[2]**

[1]Department of Mechanical, Bioresources and Biomedical Engineering, University of South Africa, Science Campus, Florida 1709, South Africa

[2]Department of Mechanical Engineering, Bioresources and Biomedical Engineering, University of South Africa, Science Campus, Florida 1709, South Africa

e-mail: echitekk@unisa.ac.za, enwercc@unisa.ac.za

Chiteka, K., Enweremadu, C. C., Coupled Thermal and Optical Impact of Dust Thermophysical Properties on Solar Photovoltaic Performance, J.sustain. dev. energy water environ. syst., 14(2), 1140695, 2026,
DOI: https://doi.org/10.13044/j.sdewes.d14.0695

ABSTRACT

Dust deposition on photovoltaic modules induces coupled optical and thermal effects that significantly reduce energy yield. This study developed an integrated computational framework combining a temperature-dependent Beer-Lambert optical model with computational fluid dynamics based thermal analysis of soiled photovoltaic modules to quantify performance losses as a function of dust thermophysical properties. Results show that transmittance decreased from 1.0 to 0.852, corresponding to a 14.8% optical loss, while surface temperature increased by 13.3 K under stagnant conditions, producing a thermal penalty of 5.3%. The combined effect yielded a total daily energy loss of 20.1% at standard irradiance. Sensitivity analysis revealed that low-conductivity dust (κ = 0.1 W/mK) and a larger dust layer caused the highest thermal rises, whereas wind speed reduced but did not eliminate insulating effects. Partitioning analysis revealed optical losses being dominant at light dust loading with 70% of total loss at 0.05 kg/m², while thermal losses rose to 45% under heavy loading of 0.20 kg/m². Losses levelled near 22% due to thermal and optical saturation. The study showed that excluding thermal effects in modelling underestimates performance degradation and the coupled model in this study provided an improved model for predicting photovoltaic yield losses that address both optical attenuation and thermal insulation.

KEYWORDS

Dust thermophysical properties, Optical transmissivity, Computational fluid dynamics, Solar PV soiling, Thermal modelling, Dust shading, Energy loss.

INTRODUCTION

Solar photovoltaics (PV) are an integral part of the global energy transition to sustainable energy technologies. Projections in literature have shown that PV may be able to supply about 10% of global electricity requirements by 2030, especially in sun-rich, arid, and semi-arid regions [1]. However, dust deposition heavily affects the performance of such solar systems in these environments. Field observations done under arid conditions have shown that intense soiling can increase optical losses by up to 70% which lead to proportional power losses [2]. Dust deposition is influenced by dust particle size, wind speed, humidity, and other environmental factors, and humidity combined with fine dust particles, and low wind speeds increase performance losses [3], [4]. Seasonal rainfall and humidity affect dust size

* Corresponding author

composition and distribution [5], while dust potency, characterised by fine and carbon-rich particles cause higher losses due to enhanced surface coverage and light scattering [6], [7].

Wind speed and relative humidity determine atmospheric dust concentration levels, and strong winds coupled with low humidity increase particle mobilization [8]. High wind speeds also increase dust removal and enhance convective cooling on solar PV modules [9]. In addition, dust in humid environments forms a hard, adherent layer that resist natural cleaning thus promoting soiling [10].

Dust deposition impacts the PV thermal behaviour through modifying the convective cooling process which raises the surface temperature, and promotes hotspot formation [11]. Accumulated dust layers act as a thermal insulator which enhances heat retention and increases hotspot severity [12]. Experimental studies have shown that thermal effects of dust are heavily reliant on its composition and materials like silica, fly ash, and cement exhibit a distinct impact on PV surface heat retention and dissipation [13]. Research also shows that heatwaves enhance these effects by promoting drier conditions, which accelerate dust accumulation and elevate module temperatures [14]. Therefore, excluding dust-induced impacts in both optical transmittance and thermal behaviour result in underprediction of solar PV performance losses [15].

The optical, thermophysical, and chemical characteristics of dust affect the optical, electrical, and thermal behaviour of PV modules [12]. For instance, silica-related surface properties affect PV optical performance by altering its reflectance, dust adhesion, and the resulting thermal impacts [16]. Islam *et al.* [17] found that the optical and thermophysical characteristics of dust significantly increase module temperature which in turn decrease electrical output. In another study, Chiteka and Enweremadu [18] showed that dust particle size, density, conductivity, and specific heat capacity can directly affect PV cell temperature and increase thermal losses.

Advanced optical–thermal models need to incorporate dust particle characteristics to correctly predict both optical and thermal impacts [19]. Finite element analysis show that crystalline silicon PV modules can develop lateral temperature gradients of up to 5 °C caused by variations in tilt, airflow dynamics, and orientation, which influence the localized heat accumulation and dissipation efficiency [20]. Three-dimensional CFD simulations have shown roof angle, wind speed, and particle size affect wind flow causing non-uniform dust deposition and efficiency losses of up to 4.1% [21]. Variations in dust elemental constituents such as Fe_2O_3, SiO_2, and carbonaceous materials significantly affects the reflectance and emissivity, which increases heat retention and module temperature [22]. Modelling studies which integrate both optical and thermal effects show that dust deposition density and particle size distribution govern transmittance loss and surface temperature rise, with even a thin dust layer (~0.224 mg/cm²) reducing PV power output by more than 13% [23]. Many existing models have relied on simplifying assumptions, and treat dust as an optical attenuator and neglecting thermophysical parameters [24]. Such simplifications often reduce the predictive accuracy limiting applicability across diverse operating conditions [25].

Mitigation strategies in literature have focused on material and design innovations to offset PV soiling and thermal degradation. Nanostructured superhydrophobic and antireflective thin films enhance solar performance by reducing dust adhesion and thermal accumulation. This offers PV efficiency improvements of up to 30% under dusty outdoor environments [26]. For instance, Mishra *et al.* [26] developed nano-silica and nano-titania antireflective superhydrophobic coatings which showed enhanced light absorption, dust repellence, and a reduction in surface temperature of approximately 2–3 °C. This led to power output gains of up to 0.48% under high irradiance. Ehsan *et al.* [27] also showed that hydrophobic nanocoatings significantly reduce soiling and thermal degradation in tropical environments, achieving surface temperature reductions of up to 10 °C. Ghosh *et al.* [28] further demonstrated that hybrid nanostructures such as TiO_2–CNT and TiO_2–ZnO composites can enhance photocatalytic cooling and self-cleaning effects thereby improving thermal stability.

Recent advances in predictive modelling have been shown to significantly improve forecasting of PV degradation under dusty conditions. Maftah *et al.* [31] used artificial neural networks to predict daily soiling ratios on PV and CSP systems and achieved superior correlations compared to linear models. Similarly, Costa Silva *et al.* [32] used advanced supervised learning algorithms, particularly multilayer perceptrons and LSTM networks, wich could accurately capture complex interactions among dust deposition, temperature, humidity, and orientation. Despite these advances, most modelling frameworks overlook critical dust properties including density, emissivity, and specific heat capacity which govern heat absorption and thermal behaviour. Improved experimental tools, including dust coupons and semi-remote weighing systems, enable more accurate dust quantification [33], but their integration into predictive models remains limited. Almukhtar *et al.* [22] empirically validated coupled models which incorporated dust properties and meteorological data, and the model had a substantially improved accuracy in temperature predictions.

Existing coupled optical–thermal modelling studies have been focusing on the effects of dust deposition on PV performance using either stand-alone optical attenuation models or CFD-based thermal analysis, treating them in isolation. For instance, Zarei and Abdolzadeh [23] developed a coupled radiative–thermal model which assumed constant optical properties, and did not consider the temperature dependence of dust extinction. Similarly, Almukhtar [22] investigated the influence of dust chemical composition on PV thermal behaviour but the optical variability was not considered. In their comprehensive review, Younis and Alhorr [24] further showed that regardless of the significant advances in optical, empirical, and CFD modelling approaches, coupled optical attenuation with thermal feedback models are still lacking. Their study emphasized that the existing models often treat them in isolation and fail to incorporate dust thermophysical properties affecting both heat transfer and irradiance attenuation. These limitations highlight a strong need for a fully integrated, temperature-sensitive optical–thermal framework to simultaneously capture the optical and thermal interactions that affect soiled PV performance.

The present study advances the understanding of PV soiling by moving beyond conventional approaches treating deposited dust as an optical attenuator only. A coupled thermal and optical modelling framework was developed to explicitly incorporate the key dust thermophysical properties into a temperature-dependent Beer–Lambert optical model coupled to a CFD-based heat transfer analysis. This integration allowed the partitioning of PV yield losses into optical and thermal components, thereby quantifying their synergistic interaction in driving performance degradation. The novelty of this work is based on its fully integrated, temperature-sensitive coupling of optical attenuation and thermal feedback, which captures how variations in dust properties simultaneously govern irradiance attenuation and module heat retention. The remainder of this manuscript is organized as follows. Section 2 discusses the materials and methods employed in the present study. Section 3 presents the results and discussion while section 4 provides the main conclusions.

MATERIALS AND METHODS

In this study, an integrated numerical approach shown in **Figure 1** was developed to appropriately quantify the coupled thermal-optical effects of dust on soiled PV module performance. Dust thermophysical and morphological properties including density (ρ), thermal conductivity (κ), specific heat capacity (c_p), and particle diameter (d_p) were used as input variables. Computational fluid dynamics (CFD) simulations were applied to determine the thermal behaviour of soiled PV modules, while an optical transmissivity model based on a temperature-dependent Beer-Lambert law evaluated light attenuation as a function of dust composition and size distribution. The two models were then coupled, to enable a unified thermal-optical analysis in which energy losses were partitioned into distinct thermal and optical contributions.

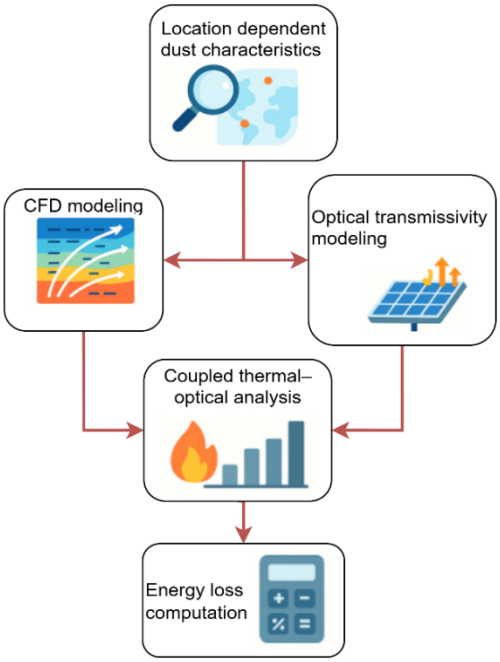

Figure 1. Methodology framework for assessing dust-induced photovoltaic performance degradation

Computational Fluid Dynamics Model

Computational Fluid Dynamics (CFD) simulations of soiled PV modules were performed, and the model incorporated dust thermophysical properties (d = 50 µm, κ = 5 W/mK, c_p = 3 kJ/kgK, ρ_d = 1800 kg/m³). The values used for these thermophysical variables were derived from reported experimental studies in literature [34]–[36]. In the present study, dust deposition on the PV surface was represented as a uniform, homogeneous layer covering the entire PV surface. The thickness of the dust layer was derived from the surface mass density and dust density. In addition to the base simulations, some selected simulations were run and these employed a non-uniform (Gaussian) deposition profile to evaluate localised thermal gradients and hotspot formation in uneven PV soiling conditions.

The computational geometry was modelled as a two-dimensional (2D) domain which was discretized with a structured mesh. This 2D domain had its dimensions defined in terms of the PV module height (H_p), representing the vertical height of the PV module above the ground. The distance from the inlet to the PV module and from the PV module to the outlet were respectively $7H_p$ and $15H_p$ and the top open boundary was $6H_p$ from the ground.

The computational domain and the boundary conditions used in the CFD simulations are illustrated in Figure 2. The left boundary was defined as a velocity inlet with a logarithmic atmospheric boundary layer profile, $u(y) = \frac{u_*}{\kappa} \ln\left(\frac{y+y_0}{y_0}\right)$, where u_* is the friction velocity, $\kappa = 0.41$ is the von Kármán constant, and y_0 is the surface roughness length. This profile represented a realistic near-ground wind flow behaviour over the PV installation site. The right boundary was specified as a pressure outlet to allow fully developed flow to exit the domain, while the top boundary was modelled as an open pressure outlet to simulate an unconfined flow field. The ground and PV panel surfaces were taken as stationary no-slip walls, with the latter representing the soiled PV surface. The inlet air temperature was set to 300 K, and the panel surface temperature was obtained from the coupled thermal–optical solution.

A 2D structured mesh was applied, and a grid independence study was performed as shown in Figure 3. The predicted temperature represented the area-averaged PV surface temperature obtained from the steady-state CFD results, ensuring that the grid independence analysis was based on an integral thermal quantity rather than a single-point value. The grid independence

results indicated that further refinement beyond 40×10^4 grid size only changed surface temperatures by <1%. As such, a grid size of 40×10^4 was used in the CFD simulations.

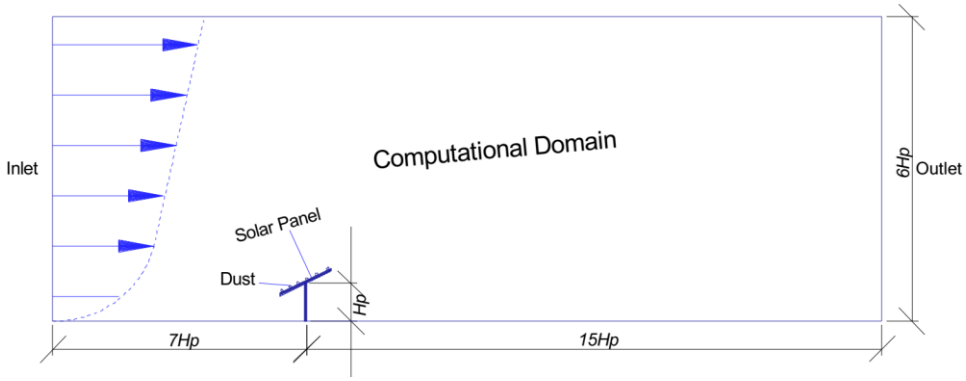

Figure 2. Computational domain

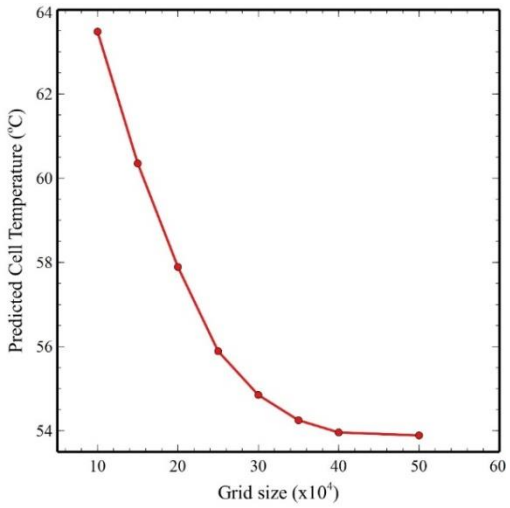

Figure 3. Grid independency study

The governing equations solved in the CFD model (ANSYS FLUENT, v2020 R2) included the steady-state Reynolds-Averaged Navier-Stokes (RANS) equations for fluid flow and the energy equation for heat transfer. The airflow was assumed to be steady, incompressible, and Newtonian, and turbulence effects were modelled using a RANS eddy-viscosity approach based on the *k–ω* turbulence model. The resulting governing momentum equation [eq. (1)] is consistent with the derivations presented in literature [37], [38]:

$$\rho(\overline{\boldsymbol{u}}\cdot\boldsymbol{\nabla})\overline{\boldsymbol{u}} = -\nabla\bar{p} + \nabla\cdot\{(\mu+\mu_t)[\nabla\overline{\boldsymbol{u}} + (\nabla\overline{\boldsymbol{u}})^{\mathrm{T}}]\} \quad (1)$$

where $\bar{u}$ denotes the Reynolds-averaged velocity vector and ρ is the fluid density; $\rho(\overline{\boldsymbol{u}}\cdot\nabla)\overline{\boldsymbol{u}}$ is the convective acceleration; $\nabla\bar{p}$ is the mean pressure gradient force per unit volume, where $\bar{p}$ is the Reynolds-averaged pressure. The term $\nabla\cdot\{(\mu+\mu_t)[\nabla\overline{\boldsymbol{u}} + (\nabla\overline{\boldsymbol{u}})^{\mathrm{T}}]\}$ represents the combined viscous and turbulent diffusion of momentum in which μ is the molecular dynamic viscosity, while μ_t is the turbulent viscosity. In this study, the *k–ω* model was used, where $\mu_t = \rho k/\omega$. The use of the *k–ω* model was due to its reliable near-wall resolution. The energy equation governing heat transfer in the system is expressed as shown by eq. (2) obtained from

the Reynolds-averaged energy equation by modelling the turbulent heat flux using a gradient diffusion approximation, following the approach of [39]:

$$\rho c_{\mathrm{a}} u_{\mathrm{j}} \frac{\partial T}{\partial x_{\mathrm{j}}} = \frac{\partial}{\partial x_{\mathrm{j}}}\left[(k + k_{\mathrm{t}}) \frac{\partial T}{\partial x_{\mathrm{j}}}\right] \tag{2}$$

$$\delta_{\mathrm{d}} = \frac{\sigma_{\mathrm{d}}}{\rho_{\mathrm{d}}} \tag{3}$$

$$q''_{\mathrm{conv}} = h(T_{\mathrm{s}} - T_{\mathrm{a}}) \tag{4}$$

where $k + k_{\mathrm{t}}$ represents the effective thermal conductivity accounting for both molecular and turbulent heat diffusion. k_{t} is the turbulent thermal conductivity, modelled as $k_{\mathrm{t}} = \frac{\mu_{\mathrm{t}} c_{\mathrm{a}}}{Pr_{\mathrm{t}}}$. In this study, μ_{t} and Pr_{t} are respectively the turbulent viscosity and the turbulent Prandtl number, taken as 0.85. c_{a} is the specific heat capacity of air (J/kgK), T (K) is temperature, and the dust layer thickness, δ_{d} was determined from the surface mass density, σ_{d} and dust density ρ_{d} according to eq. (3) and was used to represent the dust deposit as a homogeneous thermal layer in the CFD model. Dust thermophysical properties governed heat transfer within this layer, while the particle diameter d_{p} was introduced solely in the optical model to determine the extinction coefficient and size parameter governing radiative attenuation.

Boundary conditions included a constant solar irradiance G (1000 $\mathrm{W/m^2}$) on the module surface and convective heat transfer to ambient air, modelled as in eq. (4) [40], where h is the convective heat transfer coefficient, T_{s}(K) is the module surface temperature, and T_{a}(K) is the ambient air temperature. The convective heat transfer coefficient h was not prescribed a priori or calculated using empirical correlations. Instead, it emerged implicitly from the CFD solution, as it depends on the resolved near-wall velocity, turbulence, and temperature fields obtained from the coupled momentum and energy equations. To represent the insulating effect of the dust layer, the effective thermal conductivity k_{eff} at the dust-covered surface was modified as $k_{\mathrm{eff}} = \frac{k_{\mathrm{dust}}}{\delta_{\mathrm{d}}}$, where k_{dust}(W/mK) is the thermal conductivity of the dust layer. Eq. (2) – eq. (4) were coupled through boundary and source-term interactions within the CFD – optical framework. Eq. (2) is the energy equation that governs the temperature field of the PV module and dust layer. This temperature output serves as an input to eq. (4), which defines the convective heat flux at the module–air interface, and influences heat dissipation. Simultaneously, eq. (3) links the dust layer thickness derived from mass loading to the effective thermal conductivity term in eq. (2), modifying the heat transfer path. Thus, the temperature solution from eq. (2) dynamically affects both the convective boundary condition [eq. (4)] and the optical transmittance model. Air properties were modelled as temperature-dependent and the thermophysical properties of the dust layer were assumed to be constant, as their variation within the simulated temperature range is negligible. The CFD solver employed second-order spatial discretization while the Semi-Implicit Method for Pressure-Linked Equations (SIMPLE) algorithm was adopted for its robustness and computational efficiency in handling pressure‑velocity coupling in incompressible flows. Iterations ran until a residual threshold of 10^{-6} was achieved for all governing equations.

The aerodynamic validation of the CFD model was conducted against experimental data by Tominaga and Blocken [41] (**Figure 4**), which involved wind tunnel experiments under a neutral atmospheric boundary layer. In their study, velocity and pressure data were provided

although thermal measurements were not provided. However, convective heat transfer in the CFD model is governed by the local velocity field and turbulence characteristics. This meant that accurate prediction of the flow behaviour meant that the corresponding convective heat flux and surface temperature distributions were physically consistent. Therefore, the validation of the aerodynamic field provided a reasonable foundation for the reliability of the coupled thermal–optical model. In **Figure 4**, H denotes the vertical height above the ground within the computational domain, corresponding to the position where flow velocity (U_{H}) is evaluated along the logarithmic atmospheric boundary layer profile. The validation exercise revealed a mean deviation of 3.2% between the simulated and experimental surface temperatures.

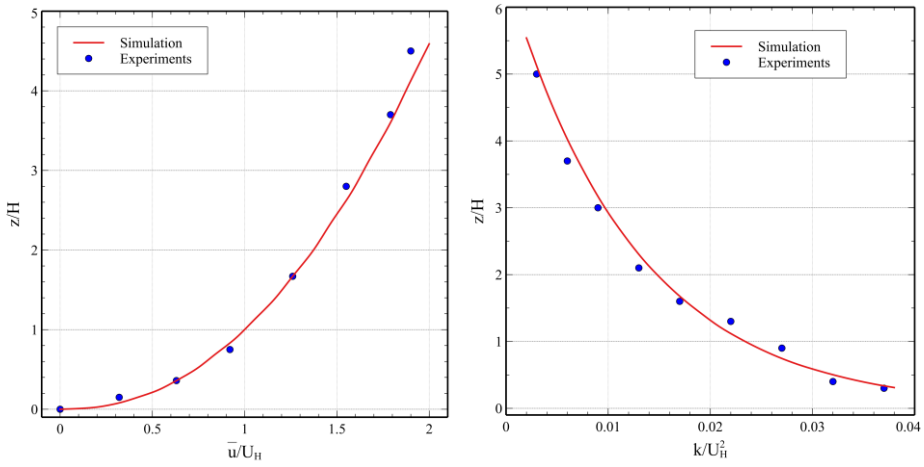

(a) (b)

Figure 4. Comparison of experimental measurements and Computational Fluid Dynamics simulation results for the incident profiles of (a) normalized mean velocity $\bar{u}/U_{\mathrm{H}}$ and (b) normalized turbulent kinetic energy k/U_{H}^2 as a function of the dimensionless height z/H

Optical Modelling

The optical performance degradation of PV modules was quantified using the Beer-Lambert law, which describes the reduction in transmittance of soiled PV glass by incorporating both scattering and absorption as functions of dust properties and layer thickness. The transmittance (τ) of the dust-covered surface is given by eq. (5) [42], where β_{e} [43] is the extinction coefficient of the dust layer and δ_{d} is the dust layer thickness determined from mass loading:

$$\tau = e^{(-\beta_{\mathrm{e}}\delta_{\mathrm{d}})} \tag{5}$$

$$\beta_{\mathrm{e}} = Q_{\mathrm{e}}\frac{3}{4}\frac{1}{d_{\mathrm{p}}}\phi \tag{6}$$

$$\beta_{\mathrm{e}}(T_{\mathrm{s}}) = \beta_{\mathrm{e},0}[1 + \alpha_{\mathrm{T}}(T_{\mathrm{s}} - T_0)] \tag{7}$$

$$\eta(T_{\mathrm{s}}, \tau) = \eta_0[1 - \sigma(T_{\mathrm{s}} - T_0)]\tau \tag{8}$$

β_e was expressed in terms of dust particle properties through the extinction efficiency factor (Q_e), as shown in eq. (6). Here, d_p is the mean particle diameter and ϕ is the volume fraction of dust. The factor Q_e depends on the size parameter $x = \frac{\pi d_p}{\lambda}$ [44], which relates particle size to the wavelength (λ) of incident light. For the representative dust particle diameter adopted in this study ($d_p = 50$ μm) and a single effective wavelength of $\lambda = 0.55$ μm, corresponding to standard solar irradiance conditions (1000 W/m²), an optical size parameter of $x \approx 2.85 \times 10^2$ was used in this study. For the spherical particles considered in this study, Q_e was calculated using Mie theory. To capture the effect of temperature, the extinction coefficient was further modelled as a function of surface temperature (T_s), accounting for changes in refractive index and emissivity of dust under solar loading. This temperature dependence is expressed in eq. (7), where $\beta_{e,0}$ is the extinction coefficient at the reference temperature, T_0 and α is the temperature sensitivity coefficient of extinction. The relationship between module efficiency (η), surface temperature (T_s), and transmittance (τ)was described by $\eta(T_s, \tau) = \eta_0[1 - \sigma(T_s - T_0)]$ [45] and in the present work, this relation was further extended to include the optical transmittance factor τ, accounting for optical losses, yielding eq. (8). In this expression, η_0 represents the reference module efficiency under clean conditions at T_0, while σ is the temperature coefficient of efficiency.

Energy Computations

Energy loss due to dust accumulation was quantified using an integrated framework partitioning total yield reduction into optical and thermal components. The instantaneous power output of a dust-laden module was expressed as in eq. (9), where the efficiency $\eta(T_s, \tau)$ depends on surface temperature and optical transmittance, $G(t)$ is the incident solar irradiance, and A is the active module area. The daily energy yield under dusty conditions was obtained by integrating instantaneous power over the day, as shown in eq. (10). For comparison, the clean module yield was defined under dust-free conditions with nominal efficiency η_0 given in eq. (11):

$$P_d(t) = \eta[T_s(t), \tau(t)]\, G(t)\, A \tag{9}$$

$$E_d = \int_0^{t_f} P_d(t)\, dt \tag{10}$$

$$E_0 = \int_0^{t_f} \eta_0\, G(t)\, A\, dt \tag{11}$$

$$\Delta E = E_0 - E_d \tag{12}$$

The total energy loss attributable to dust was then computed as the difference between clean and dust-laden yields, as defined in eq. (12). To separate the effects, optical loss was calculated from transmittance reduction alone, expressed as $\Delta E_\tau = E_0 - E_d$, while thermal loss was determined as $\Delta E_T = E_\tau - E_d$, where E_τ accounts only for dust-induced reduction in transmittance and E_d incorporates both optical and thermal effects.

RESULTS AND DISCUSSION

The thermal behaviour of dust-laden photovoltaic modules was examined using CFD simulations to compute the surface temperature rise under representative operating conditions. A sensitivity analysis was then carried out to assess the influence of dust thermophysical properties and environmental parameters, including wind speed and dust layer characteristics, on thermal performance of the PV module. The optical attenuation and thermal penalties were then combined to determine total energy yield losses, with particular emphasis on partitioning the relative contributions of optical and thermal effects and identifying saturation behaviour under heavy dust loading.

Computational Fluid Dynamics Simulation Results

The CFD simulations revealed that dust accumulation significantly alters the thermal performance of PV modules. Under clean-surface conditions, the module exhibited nearly uniform surface temperatures ranging from 321 K to 322 K. However, the addition of a representative dust layer characterized by a particle diameter of 50 μm, thermal conductivity of 5 W/mK, specific heat capacity of 3 kJ/kgK, and density of 1800 kg/m³, increased the peak surface temperature to 335.1 K under an irradiance of 1000 W/m² (see **Figure 5**). This 13.3 K rise corresponds to a wind speed of 0 m/s (i.e., natural convection only), which served as the baseline condition for all subsequent sensitivity simulations. This temperature rise resulted in a 5.3% loss in power output considering a −0.5%/K temperature coefficient of performance for crystalline silicon PV modules.

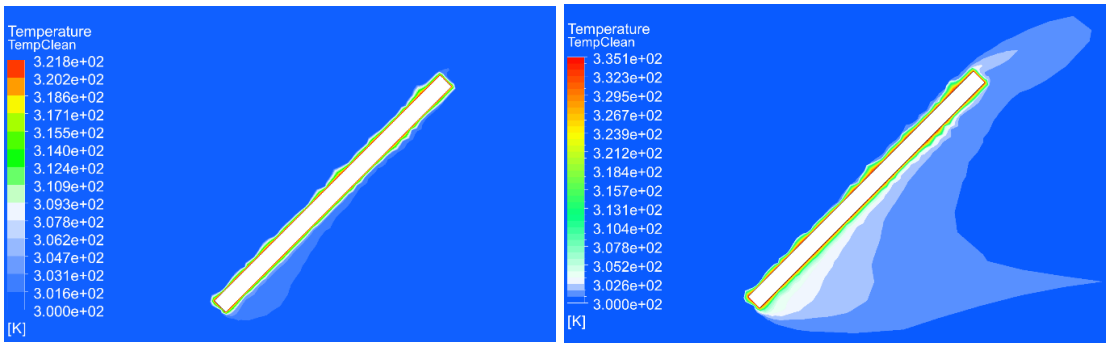

(a) (b)

Figure 5. CFD temperature contours of PV module (a) clean surface, (b) dust-loaded surface

The insulating nature of the dust layer was the primary contributor to the performance degradation of the PV module. A reduction in the effective thermal conductivity of the PV surface caused dust impeding heat dissipation to the ambient environment, thus elevating surface temperatures. This thermal resistance lead to steep temperature gradients promoting localized hotspots. As shown in **Figure 5**, these effects are visible in the simulated temperature contours. **Figure 5** shows both the PV module surface temperature and the surrounding fluid temperature field, which shows the development of a thermal gradient on the heated PV surface. The analysis of velocity vectors indicated that the dust used in this study had a negligible effect on flow separation and turbulence intensity. This shows that that thermal insulation and not aerodynamic drag, was responsible for the elevated temperatures.

Sensitivity Analysis of Dust Thermophysical Properties and Environmental Parameters

A sensitivity analysis was carried out to assess the suitability of the CFD model under different operating conditions, relative to a defined base case representing typical soiled PV operating conditions. A base case was developed with a wind speed and dust layer thickness of

respectively 0 m/s, and 50 μm. This was coupled with a thermal conductivity of 1 W/mK, uniform dust deposition, and an ambient temperature of 300 K under a constant solar irradiance of 1000W/m^2 applied to the module surface. Parametric variations of the wind speed, thermal conductivity, and dust layer thickness were performed independently while holding all other parameters fixed at the base case values. The module temperature was evaluated as the area-averaged photovoltaic module surface temperature obtained from the steady-state CFD solution.

Wind speed was varied between 0 and 5 m/s, corresponding to increases in the convective heat transfer coefficient from approximately 10 to 45 W/m²K. Here, wind speed refers to the inlet velocity evaluated at the photovoltaic module height from the prescribed atmospheric boundary layer profile. Results indicated that the surface temperature rise decreased from 13.3 K at 0 m/s to 8.5 K at 2 m/s, and further down to 6.1 K at 5 m/s. It was revealed that higher wind speeds improve convective cooling although it does not fully eliminate the insulating effect of the dust layer.

κ was evaluated from 0.1 to 10 W/mK to analyse the effect of dust thermal conductivity (κ) on temperature. An inverse relationship was noticed from the simulations and lower-conductivity dust particles produced higher temperature rises owing to their stronger insulating effect (**Figure 6**). For instance, at κ = 0.1 W/mK, representative of soot or fly ash, the surface temperature increase reached 16.8 K, whereas at κ = 10 W/mK, typical of metallic oxides, the rise was 5.4 K highlighting the critical influence of dust mineralogy on thermal loading (see **Table 1**).

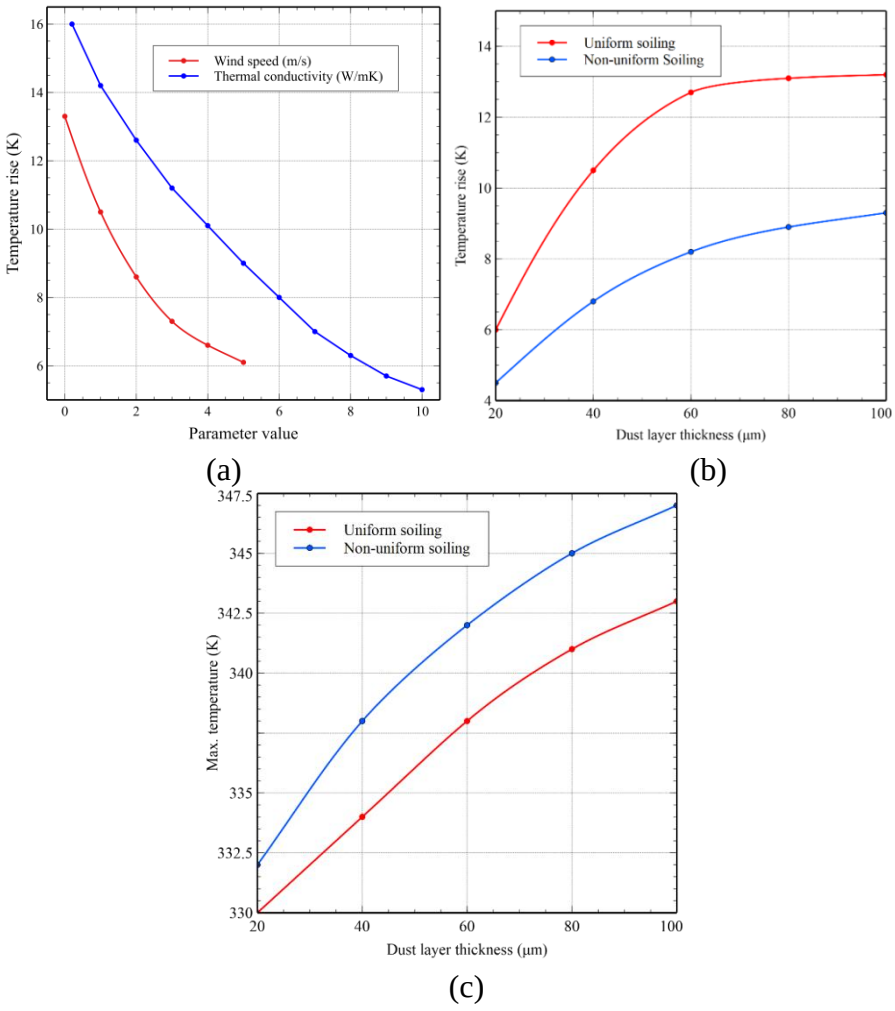

Figure 6. Sensitivity Analysis of (a) wind speed and thermal conductivity, and (b) dust layer thickness

Table 1. Parameter sensitivity analysis

Parameter Varied	Range Tested	Temperature Rise (K)	Key Insight
Wind Speed (m/s)	0 – 5	Reduced from 13.3 K to 6.1 K	Increased airflow mitigates thermal insulation
Dust Thermal Conductivity (W/mK)	0.1 – 10	Reduced from 16.8K to 5.4 K	Low-κ dusts trap more heat
Dust Layer Thickness (μm)	20 – 100	Increased until 60 μm, then plateau at 13.2 K	Thermal saturation beyond critical thickness
Deposition Uniformity	Uniform vs. Gaussian	Local peak in temperature up to 340 K	Uneven soiling promotes hotspots and thermal stress

Both area-averaged photovoltaic module surface temperature rise and the maximum temperature measured at the hottest spot on the photovoltaic module surface were used in the assessment of thermal behaviour under different soiling patterns. These assessments were done for both uniform and non-uniform dust deposition (**Figure 6b** and **Figure 6c**). The area-averaged temperature rise characterised the global thermal response relevant to power performance. On the other hand, the hottest-spot temperature reflects localized thermal stress, occurring at a dust-induced hotspot for non-uniform deposition and at the hottest surface location under uniform dust coverage. Dust layer thickness was varied from 20 to 100 μm to simulate different levels of dust particle sizes. The results showed that temperature rise increased from 6.0 K at 20 μm to 13.2 K at 100 μm, but the rate of increase plateaued beyond 60 μm, indicating thermal saturation. This implied a limit beyond which additional dust thickness does not meaningfully increase thermal resistance. An analysis of a non-uniform (Gaussian) dust profile, simulating more realistic field conditions revealed localized hotspots with surface temperatures exceeding 340 K, despite average temperatures being 8 – 10 K above clean-module levels. Under real operating conditions, such gradients pose a risk for encapsulant degradation and mechanical fatigue.

Coupled Thermal-Optical Effects and Energy Yield Loss Quantification

In the optical analysis, transmittance dropped from 1.0 to 0.852, corresponding to a 14.8% reduction in irradiance incident on the PV surface. When combined with the 13.3 K thermal rise which translates to a 5.3% efficiency loss, the total daily energy yield reduction reached about 20.1% under uniform dust coverage at 1000 W/m² at −0.5%/K temperature coefficient of crystalline silicon modules. The magnitude of the thermal loss was in line with the CFD results showing that the observed efficiency reduction is not purely a function of shading but also of dust-induced heat retention. The modelled 20.1% efficiency reduction aligns well with experimental observations. For instance, Rashid *et al.* **[35]** reported a 15 – 25% efficiency losses for polycrystalline PV modules under natural dust densities of 6.4 – 10.3 g/m², which was accompanied by temperature rises of up to 5 °C. Another study by Almukhtar *et al.* **[17]** also reported similar results in which they observed 5 – 18% power losses and module temperature increases of up to 12 °C depending on dust type and thickness.

Partitioning analysis demonstrated in **Figure 7** further reveals the shifting dominance of the two mechanisms. In this analysis with a light dust loading of approximately 0.05 kg/m^2, optical attenuation accounted for about 70% of the total loss, whereas at higher loading of approximately 0.20 kg/m^2, thermal effects contributed as much as 45%. This pattern reflects the progressive suppression of convective cooling as dust layers thicken, reinforcing the results from sensitivity analysis where low-conductivity and thick dust deposits produced the highest temperature rises. Furthermore, the dust-induced temperature elevation had an effect of

increasing the extinction coefficient, slightly worsening optical attenuation, thus creating a feedback loop between heating and light loss.

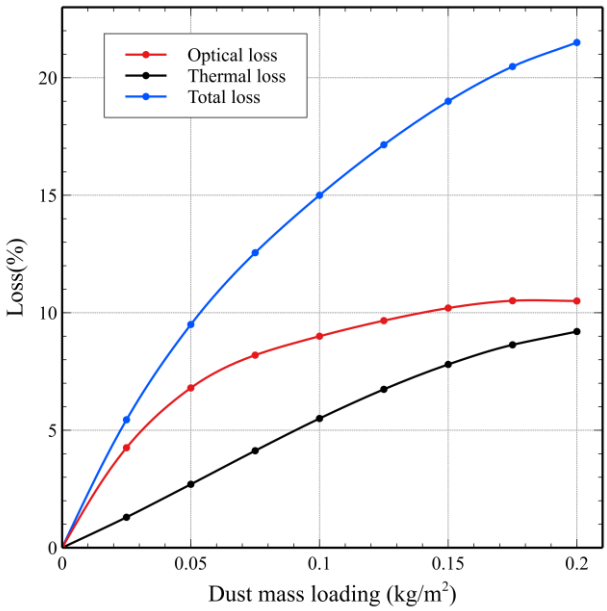

Figure 7. Variation of optical,thermal, and total energy loss with dust mass loading on photovoltaic module surfaces

The plateau effect was noted beyond 0.20 kg/m² in the coupled analysis where yield reduction longer grew proportionally with mass loading. This saturation effect was explained by the thermal saturation behaviour in which once a critical dust thickness is reached, additional layers no longer significantly impede heat dissipation but still maintain high optical blockage. As a result, energy losses stabilised at about 22%, suggesting that extreme soiling may not produce proportionally higher yield penalties beyond a certain threshold. However, this was dependent on the dust particle type. Therefore, the results in this study indicate that the coupling of thermal and optical processes emphasizes the importance of dust mineralogy where fine, low-conductivity particles such as soot or fly ash are mostly harmful since they both block irradiance and trap heat.

CONCLUSIONS

In this study, a coupled thermal-optical framework was developed to analyse PV performance degradation under PV soiling, incorporating dust thermophysical properties. The results revealed that dust cause dual penalties which include a direct reduction in transmittance and an indirect thermal impact due to its insulating effect. The CFD simulation runs revealed that surface temperatures increased by up to 13.3 K under stagnant conditions, leading to a thermal efficiency penalty of about 5.3%. Sensitivity analysis showed that low-conductivity dust (κ = 0.1 W/mK) and thicker layers caused the greatest thermal rise, while wind speed partially mitigated although it did not eliminate the insulating effect.

The optical model showed a 14.8% irradiance loss caused by reduced transmittance, and when combined with the thermal losses, produced an overall energy yield reduction of about 20.1% under standard irradiance. Partitioning analysis revealed that optical effects dominated at light dust loading with 70% of total loss at 0.05 kg/m^2. However, thermal effects were significant at higher dust loading with up to 45% at 0.20 kg/m$^{2.}$ This shows the synergistic interactions between optical attenuation and thermal insulation, in which dust-induced heating further increased the extinction coefficient thereby strengthening the optical losses. A saturation

trend was observed beyond 0.20 kg/m^2, with energy yield losses plateauing near 22% due to both thermal and optical saturation.

This study shows that neglecting thermal effects leads to a significant underestimation of PV yield losses, particularly in hot, arid regions where fine and low-conductivity dust such as soot or fly ash are common. The present work explains the importance of dust mineralogy and morphology in determining soiling severity and set the base line for mitigation strategies tailored to both optical and thermal impacts. Future research work may incorporate heterogeneous dust deposition, humidity effects, and temperature-dependent dust properties to further improve the predictive accuracy, which in turn improve PV system reliability across diverse environments.

NOMENCLATURE

Symbols

A	active module area	[m²]
c_p	specific heat capacity	[J/kgK]
c_a	specific heat capacity of air	[J/kgK]
d_p	dust particle diameter / mean dust particle diameter	[m]
$G(t)$	incident solar irradiance	[W/m²]
h	convective heat transfer coefficient	[W/m²K]
k_{eff}	effective thermal conductivity of dust-covered surface	[W/mK]
$\bar{p}$	Reynolds-averaged pressure	[Pa]
Q_e	extinction efficiency factor	[-]
q''_{conv}	convective heat flux	[W/m²]
T	temperature	[K]
T_a	ambient air temperature	[K]
T_s	PV module surface temperature	[K]
T_0	reference temperature	[K]
$\bar{u}$	Reynolds-averaged velocity vector	[m/s]

Greek letters

α	temperature sensitivity coefficient of extinction	[K^{-1}]
κ	thermal conductivity	[W/mK]
σ_d	surface mass density of dust	[kg/m²]
δ_d	dust layer thickness	[m]
ρ	air density	[kg/m³]
ρ_d	dust density	[kg/m³]
ϕ	volume fraction of dust	[-]
η	module efficiency	[%]
η_0	nominal reference efficiency at T_o (%)	[%]
τ	optical transmittance	
β_e	extinction coefficient	[m^{-1}]
$\beta_{e,0}$	reference extinction	[m^{-1}]

	coefficient at T_o (m^{-1})	
$\beta_e(T_s)$	temperature-dependent extinction coefficient (m^{-1})	[m^{-1}]
σ	temperature coefficient of efficiency	[%/K]
ΔE	total energy yield loss	[%]
ΔE_τ	optical energy loss	[%]
ΔE_T	thermal energy loss	[%]
λ	wavelength of incident light	[µm]
μ	molecular dynamic viscosity	[Pa·s]
μ_t	turbulent viscosity	[Pa·s]
x	optical size parameter	[-]
$\nabla\bar{p}$	mean pressure gradient force per unit volume	[Pa/m]

Abbreviations

AI	Artificial Intelligence
ANN	Artificial Neural Network
BIPV	Building-Integrated Photovoltaics
CFD	Computational Fluid Dynamics
CPV	Concentrating Photovoltaics
CRediT	Contributor Roles Taxonomy
FEM	Finite Element Method
ML	Machine Learning
PV	Photovoltaic
RANS	Reynolds-Averaged Navier-Stokes
SIMPLE	Semi-Implicit Method for Pressure-Linked Equations

REFERENCES

1. Garg A., Sarojwal A., Sharma D.D., Probing the Impact of Dust on Solar Photovoltaic Performance Using Cutting Edge Techniques for Performance Optimization, *2024 IEEE Region 10 Symposium (TENSYMP)*, 2024, pp 1–7, https://doi.org/10.1109/TENSYMP61132.2024.1052232.
2. Li M., Colvin D., Gao M, Gorricho A., Seigneur H., Impact of Soiling on PV Modules and Strings of Field-Exposed PV Systems, *2021 IEEE 48th Photovoltaic Specialists Conference (PVSC)*, 2021, pp 1466–7, https://doi.org/10.1109/PVSC43889.2021.9518429.
3. Zhao W, Lv Y, Zhou Q, Yan W. Investigation on particle deposition criterion and dust accumulation impact on solar PV module performance, *Energy*; Vol. 233, 121240, 2021, https://doi.org/10.1016/j.energy.2021.121240.
4. El Alani O., Abraim M., Ghennioui H., Ghennioui A., Azouzoute A., Evaluation of Aerosols Impact on global and direct irradiance attenuation under clear sky condition: A case study in Morocco, *Journal of Sustainable Development of Energy, Water and Environment Systems*, Vol. 11, No. 1, 1100433, 2023, https://doi.org/10.13044/j.sdewes.d10.0433.
5. Valerino M., Ratnaparkhi A., Ghoroi C., Bergin M., Seasonal photovoltaic soiling: Analysis of size and composition of deposited particulate matter, *Solar Energy*, Vol. 227, pp 44–55, 2021, https://doi.org/10.1016/j.solener.2021.08.080.
6. Javed W., Guo B., Figgis B., Aïssa B., Dust potency in the context of solar photovoltaic (PV) soiling loss. *Solar Energy*, Vol. 220, pp 1040–1052, 2021, https://doi.org/10.1016/j.solener.2021.04.015.

7. Fan S., Wang Y., Cao S., Sun T., Liu P., A novel method for analyzing the effect of dust accumulation on energy efficiency loss in photovoltaic (PV) system. *Energy*, Vol. 234, 121112, 2021, https://doi.org/10.1016/j.energy.2021.121112.
8. Csavina J., Field J., Félix O., Corral-Avitia A.Y., Sáez A.E., Betterton E.A., Effect of wind speed and relative humidity on atmospheric dust concentrations in semi-arid climates. *Science of The Total Environment*, Vol. 487, pp 82–90, 2014, https://doi.org/10.1016/j.scitotenv.2014.03.138.
9. Salimi H., Mirabdolah Lavasani A., Ahmadi-Danesh-Ashtiani H., Fazaeli R., Effect of dust concentration, wind speed, and relative humidity on the performance of photovoltaic panels in Tehran. Energy Sources, Part A: Recovery, *Utilization, and Environmental Effects*, Vol. 45, pp 7867–7877, 2023, https://doi.org/10.1080/15567036.2019.1677811.
10. Zlateva P., Terziev A., Yordanov K., Ivanov M., Stankov B., Influence of Limestone Dust on PV Panel Efficiency in a Small Solar Park in Bulgaria. Eng, Vol. 6, 10, 2025, https://doi.org/10.3390/eng6010010.
11. Islam M.d.I., Jadin M.S., Mansur A.A., Impact of Dust Deposition on PV Performance and Hotspot Generation: I-V and Thermal Analysis with SEM and UV-VIS-NIR, *2024 IEEE 14th International Conference on Control System, Computing and Engineering (ICCSCE)*, pp 118–23, 2024, https://doi.org/10.1109/ICCSCE61582.2024.10696246.
12. Almukhtar H., Lie T.T., Al-Shohani W.A.M., Anderson T., Al-Tameemi Z., Comprehensive Review of Dust Properties and Their Influence on Photovoltaic Systems: Electrical, Optical, Thermal Models and Experimentation Techniques, *Energies*, Vol. 16, 3401, 2023, https://doi.org/10.3390/en16083401.
13. Bhattacharya S., Sadhu P.K., Singh N.K., Effect of soiling loss in solar photovoltaic modules and relation with particulate matter concentration in nearby mining and industrial sites, *Microsystem Technologies*, Vol. 31, pp 1833–1847, 2025, https://doi.org/10.1007/s00542-024-05811-y.
14. Al-Baghdadi M.A.R.S., Impact of world's heat and dust waves on the performance and economics of photovoltaic solar energy projects, *International Journal of Energy, Environment, and Economics*, Vol. 30, pp 227–250, 2022.
15. Barth N., Figgis B., Abdallah A.A., Aly S.P., Ahzi S., Figgis B., Modeling of the Influence of Dust Soiling on Photovoltaic Panels for Desert Applications: The Example of the Solar Test Facility at Doha, Qatar, *2017 International Renewable and Sustainable Energy Conference (IRSEC)*, 2017, pp 1–6, https://doi.org/10.1109/IRSEC.2017.8477249.
16. Thomas K., Rahman A. et al., Optimizing Light Management in Bifacial Perovskite Solar Cells Using Silica Based Anti-Dust and Anti-Reflection Coatings for Harsh Environments, *Processes*, Vol. 13, No. 2, 578, 2025, https://doi.org/10.3390/pr13020578.
17. Almukhtar H., Lie T.T., Al-Shohani W.A.M., Comprehensive analysis of dust impact on photovoltaic module temperature: Experimental insights and mathematical modeling, *Solar Energy*, Vol. 265, 112125, 2023, https://doi.org/10.1016/j.solener.2023.112125.
18. Chiteka K., Enweremadu C.C., Investigating the influence of dust particle thermophysical properties on soiled solar cell temperature, *Case Studies in Thermal Engineering*, Vol. 64, 105407, 2024, https://doi.org/10.1016/j.csite.2024.105407.
19. Hooshyar P., Moosavi A., Borujerdi A.N., Enhanced dust reduction method for solar panels application, *Scientific Reports*, Vol. 14, 30351, 2024, https://doi.org/10.1038/s41598-024-81183-7.
20. Tomšič Š., Lipovšek B., Bokalič M., Topič M., Unraveling Temperature Distribution Within Crystalline Silicon PV Modules by Different Finite Element Method-Based Thermal Modeling Approaches, *Advanced Theory and Simulations*, Vol. 8, 2401026, 2025, https://doi.org/10.1002/adts.202401026.

21. Peng H., Lu H., Chang X., Zheng C., Wang Y., 3D CFD modelling of dust deposition characteristics and influences on building-mounted photovoltaic system, *Case Studies in Thermal Engineering*, Vol. 35, 102138, 2022, https://doi.org/10.1016/j.csite.2022.102138.
22. Almukhtar H., The Role of Accumulated Dust Chemical Composition on Photovoltaic Thermal Performance: Advanced Modeling and Experimental Analysis, *PhD Thesis*, Auckland University of Technology, 2024.
23. Zarei T., Abdolzadeh M., Optical and thermal modeling of a tilted photovoltaic module with sand particles settled on its front surface, *Energy*, Vol. 95, pp 51–66, 2016, https://doi.org/10.1016/j.energy.2015.11.045.
24. Younis A., Alhorr Y., Modeling of dust soiling effects on solar photovoltaic performance: A review, *Solar Energy*, Vol. 220, pp 1074–1088, 2021, https://doi.org/10.1016/j.solener.2021.04.011.
25. Sharma S., Malik P., Sinha S., The impact of soiling on temperature and sustainable solar PV power generation: A detailed analysis, *Renewable Energy*, Vol. 237, 121864, 2024, https://doi.org/10.1016/j.renene.2024.121864.
26. Mishra A., Gill F.S., Bhatt N., Rathod A.P.S., Rajput A., Fabrication of antireflective superhydrophobic coating for self-cleaning solar panels and study of energy efficiency, *Physics of Fluids*, Vol. 36, 017111, 2024, https://doi.org/10.1063/5.0180015.
27. Ehsan R.M., Simon S.P., Sundareswaran K., Kumar K.A., Sriharsha T., Effect of Soiling on Photovoltaic Modules and Its Mitigation Using Hydrophobic Nanocoatings, *IEEE Journal of Photovoltaics*, Vol. 11, pp 742–749, 2021, https://doi.org/10.1109/JPHOTOV.2021.3062023.
28. Ghosh A., Chakraborty R., Das A., Kumar A., Abating air pollution using nanoparticles and sustainable technologies through holistic lens, *Nanotechnology for Environmental Engineering*, Vol. 9, pp 637–677, 2024, https://doi.org/10.1007/s41204-024-00388-3.
29. Zaini F., Synthesis and Characterization of Hybrid Organic Coating System to Reduce Thermal Degradation of Solar Cells, *Master's Thesis*, University of Malaya, 2020.
30. Kale P.G., Singh K.K., Seth C., Modeling Effect of Dust Particles on Performance Parameters of the Solar PV Module, *2019 Fifth International Conference on Electrical Energy Systems (ICEES)*, pp 1–5, 2019, https://doi.org/10.1109/ICEES.2019.8719298.
31. Maftah A., Azouzoute A., El Ydrissi M., Oufadel A., Maaroufi M., Soiling investigation for PV and CSP system: experimental and ANN modelling analysis in two sites with different climate, *International Journal of Sustainable Energy*, Vol. 41, pp 629–645, 2022, https://doi.org/10.1080/14786451.2021.1965605.
32. Araujo Costa Silva L., Baca Ruiz L.G., Criado-Ramón D., Gabriel Bessa J., Micheli L., Pegalajar Jiménez M. del C., Assessing the impact of soiling on photovoltaic efficiency using supervised learning techniques, *Expert Systems with Applications*, Vol. 231, 120816, 2023, https://doi.org/10.1016/j.eswa.2023.120816.
33. Aweenagua F, Isaacs S, Takyi J, Afari AA, Beem HR. Experimental Approaches for Estimating the Mass of Dust Soiling on PV Modules Using Coupons. *2024 IEEE International Conference on Artificial Intelligence & Green Energy (ICAIGE)*, 2024, p. 1–6. https://doi.org/10.1109/ICAIGE62696.2024.10776705.
34. Javed W., Guo B., Wubulikasimu Y., Figgis B.W., Photovoltaic performance degradation due to soiling and characterization of the accumulated dust, *2016 IEEE International Conference on Power and Renewable Energy (ICPRE)*, 2016, pp 580–584, https://doi.org/10.1109/ICPRE.2016.7871142.
35. Rashid M., Yousif M., Rashid Z., Muhammad A., Altaf M., Mustafa A., Effect of dust accumulation on the performance of photovoltaic modules for different climate regions, *Heliyon*, Vol. 9, e23069, 2023, https://doi.org/10.1016/j.heliyon.2023.e23069.

36. Guan Y., Zhang H., Xiao B., Zhou Z., Yan X., In-situ investigation of the effect of dust deposition on the performance of polycrystalline silicon photovoltaic modules, *Renewable Energy*, Vol. 101, pp 1273–1284, 2017, https://doi.org/10.1016/j.renene.2016.10.009.
37. Lunev V.V., Modified Version of the Averaged Navier–Stokes Equations, *Fluid Dynamics*, Vol. 54, pp 279–289, 2019, https://doi.org/10.1134/S0015462819020083.
38. Kajishima T., Taira K., Reynolds-Averaged Navier–Stokes Equations, *In: Computational Fluid Dynamics: Incompressible Turbulent Flows*, Springer, 2017, pp 237–268, https://doi.org/10.1007/978-3-319-45304-0_7.
39. Heyerichs K., Pollard A., Heat transfer in separated and impinging turbulent flows, *International Journal of Heat and Mass Transfer*, Vol. 39, pp 2385–2400, 1996, https://doi.org/10.1016/0017-9310(95)00347-9.
40. Ermolaev V., *Thermal Engineering*, Springer Nature Switzerland, 2024, https://doi.org/10.1007/978-3-031-50373-3.
41. Tominaga Y., Blocken B., Wind tunnel experiments on cross-ventilation flow of a generic building with contaminant dispersion in unsheltered and sheltered conditions, *Building and Environment*, Vol. 92, pp 452–461, 2015, https://doi.org/10.1016/j.buildenv.2015.05.026.
42. Zhong H., Li G., Tian B., Wen Y., Li W., Li T., Attenuation Characteristics of Laser Fuzes in Low-Visibility Dust Environments, 2024 14th International Symposium on Antennas, Propagation and EM Theory (ISAPE), 2024, pp 1–4, https://doi.org/10.1109/ISAPE62431.2024.10840631.
43. Nilsson T.K., Sundén B., Thermal radiative coefficients of cylindrically and spherically shaped soot particles and soot agglomerates, Heat and Mass Transfer, Vol. 41, pp 12–22, 2004, https://doi.org/10.1007/s00231-004-0519-3.
44. Sharma S.K., Light scattering and absorption characteristics of optically soft particles, In: Light Scattering Reviews, Springer, 2006, pp 73–123, https://doi.org/10.1007/3-540-37672-0_3.
45. Bayrakci M., Choi Y., Brownson J.R.S., Temperature Dependent Power Modeling of Photovoltaics, Energy Procedia, Vol. 57, pp 745–754, 2014, https://doi.org/10.1016/j.egypro.2014.10.282.

Paper submitted: 29.10.2025
Paper revised: 26.01.2026
Paper accepted: 02.02.2026